DMD Fast Forward. Published on July 14, 2014 as doi:10.1124/dmd.114.058032

Title Page

Towards a Unified Model of Passive Drug Permeation II: The Physiochemical Determinants of Unbound Tissue Distribution with Applications to the Design of Hepatoselective Glucokinase Inhibitors

Avijit Ghosh, Tristan S. Maurer, John Litchfield, Manthema V. Varma, Charles Rotter, Renato Scialis, Bo Feng, Meihua Tu, Cris R.W. Guimaraes, and Dennis O. Scott

Systems Modeling and Simulation, Department of Pharmacokinetics, Dynamics and Metabolism, Pfizer Inc. 620 Memorial Drive, Cambridge MA, 02139 (A.G. and T.S.M); Cardiovascular and Metabolic Disease Research Unit, Department of Pharmacokinetics, Dynamics and Metabolism, Pfizer Inc. 620 Memorial Drive, Cambridge MA, 02139 (J.L. and D.O.S.); Enzymology and Transporters, Department of Pharmacokinetics, Dynamics and Metabolism, Eastern Point Rd, Groton, CT, 06340 (B.F., M.V., C.R., R.S.); World Wide Medicinal Chemistry, 620 Memorial Drive, Cambridge MA, 02139 (M.T. and C.R.W.G.)

DMD Fast Forward. Published on July 14, 2014 as DOI: 10.1124/dmd.114.058032
This article has not been copyedited and formatted. The final version may differ from this version.

Running Title Page

Towards a Unified Model of Passive Drug Permeation II

Corresponding Author: Avijit Ghosh, Systems Modeling and Simulation, Department of Pharmacokinetics, Pharmacodynamics and Metabolism, Pfizer Inc. 620 Memorial Drive 02139 (424) 256-6777: E-mail: avijit@physics.drexel.edu

Number Pages: 35

Number Tables: 4

Number Figures: 8

Number References: 48

Number of Words in Abstract: 207

Number of Words in Introduction: 724

Number of Words in Discussion: 1497

Abbreviations: Bicinchoninic Acid, BCA; Dimethyl Sulfoxide, DMSO; Fetal Bovine Serum, FBS; Fraction Unbound, fu; Generalized Born- Surface Area framework, GB-SA framework; Glucokinase Activators, GKA; Human Embryonic Kidney 293, HEK-293; High-Performance Liquid Chromatography, HPLC; Unbound Tissue to Plasma ratio, Kpuu; liquid chromatography tandem mass spectrometry, LC-MS/MS; Madin-Darby Canine Kidney – Low Expression ,MDCK-LE; Non-essential Amino Acids, NEAA; Organic Anion Transporting Polypeptide, OATP; Optimized Potentials for Liquid Simulations (2005) force field, OPLS-2005 force field; (S)-6-(3-Cyclopentyl-2-(4-(trifluoromethyl)-1H-imidazol-1-yl) propanamido) nicotinic acid, PF-049; 6-[(2S)-2-(4-(cyclobutanesulfonyl)-1H-imidazol-1-yl)-3-cyclopentylpropanamido) pyridine-3-carboxylic acid, PF-051; Type 2 Diabetes Mellitus, T2DM; Trans-epithelial electrical resistance, TEER; Therapeutic Index, TI; Unstirred Water Layer, UWL; wild type, WT;

DMD Fast Forward. Published on July 14, 2014 as DOI: 10.1124/dmd.114.058032
This article has not been copyedited and formatted. The final version may differ from this version.

Abstract

In this work, we leverage a mathematical model of the underlying physiochemical properties of tissues and physicochemical properties of molecules in order to support the development of hepatoselective glucokinase activators. Passive distribution is modeled via a Fick-Nernst-Planck approach, using *in vitro* experimental data to estimate the permeability of both ionized and neutral species. The model accounts for pH and electrochemical potential across cellular membranes, ionization according to Henderson-Hasselbalch, passive permeation of the neutral species using Fick's law, and passive permeation of the ionized species using the Nernst-Planck equation. The mathematical model of the physiochemical system allows derivation of a single set of parameters governing the distribution of drug molecules across multiple conditions both *in vitro* and *in vivo*. A case study using this approach in the development of hepatoselective glucokinase activators (GKA) via Organic Anion Transporting Polypeptide (OATP) mediated hepatic uptake and impaired passive distribution to the pancreas is described. The results for these molecules indicate the permeability penalty of the ionized form is offset by its relative abundance, leading to passive pancreatic exclusion according to the Nernst-Planck extension of Fickian passive permeation. Generally, this model serves as a useful construct for drug discovery scientists to understand subcellular exposure of acids or bases using specific physiochemical properties.

DMD Fast Forward. Published on July 14, 2014 as DOI: 10.1124/dmd.114.058032
This article has not been copyedited and formatted. The final version may differ from this version.

Introduction

The glucokinase enzyme, which facilitates the phosphorylation of glucose to glucose-6-phosphate, is a key regulator of glucose homeostasis through its actions in the liver, pancreas, gut, and brain. Of these tissues, the physiological role of glucokinase in the liver and pancreas is most well understood. In hepatocytes, glucokinase determines the rate of hepatic glucose uptake and plays a key role in glycogen synthesis and the regulation of hepatic glucose production. In pancreatic β-cells, glucokinase regulates glucose-stimulated insulin secretion, whereby insulin secretion in response to glucose is amplified. Because of these important physiological roles, there has been considerable interest in the development of glucokinase activators for the treatment of type-2 diabetes mellitus (T2DM). Much of this effort has followed from the identification of small molecule activators that reduce the $S_{0.5}$ (i.e. Km of glucose) and increase the V_{max} of glucokinase through interactions at an allosteric site (Grimsby *et al.*, 2003). Although initial such glucokinase activators have demonstrated robust glucose lowering in early clinical trials, the incidence of mechanism-related hypoglycemia has posed severe challenges to the development of these agents (Matschinsky, 2013). This challenge has led to a variety of approaches to maintain efficacy while obviating hypoglycemic risk (Matschinsky, 2009; Pfefferkorn and Guzman-Perez, 2012; Pfefferkorn *et al.*, 2012; Matschinsky, 2013). From a chemical design perspective, two such approaches have been described previously, namely: (1) the design of partial activators and (2) the design of activators that preferentially distribute to the liver. Efforts related to the latter approach have provided the first oral "hepatoselective" glucokinase activators, (S)-6-(3-Cyclopentyl-2-(4-(trifluoromethyl)-1H-imidazol-1-yl) propanamido) nicotinic acid (PF-049) (Pfefferkorn *et al.*, 2012) and 6-[(2S)-2-(4-(cyclobutanesulfonyl)-1H-imidazol-1-yl)-3-cyclopentylpropanamido) pyridine-3-carboxylic acid (PF-051) (Stevens *et al.*, 2013) (Figure 1). Following continuous intravenous infusion in rats over four days, unbound liver concentrations of PF-049 and PF-051 are 5-fold greater than unbound plasma concentration (Stevens *et al.*, 2013). In the same study, substantial exclusion from the pancreas and muscle was observed with unbound tissue-to-plasma ratios (*Kpuu*) of ≤ 0.17. The net effect of liver uptake and pancreatic exclusion provides liver-to-pancreas selectivity of greater than 60-fold (Figure 2).

DMD Fast Forward. Published on July 14, 2014 as DOI: 10.1124/dmd.114.058032
This article has not been copyedited and formatted. The final version may differ from this version.

On a mechanistic level, the substantial hepatic uptake of this activator was achieved by selecting molecules with affinity for active hepatic uptake via OATP1B1 and OATP1B3. However, the mechanisms underpinning the observed distributional impairment to the pancreas and muscle are less obvious. The possibility of active efflux from both the pancreas and muscle is highly unlikely. In addition, although both compounds have relatively poor permeability at physiological pH (transcellular permeability $\leq 1.5 \times 10^{-6}$ cm/s), this attribute alone cannot be used in a first principles explanation of distributional impairment to a non-clearing organ at equilibrium according to Fick's first law of diffusion. A perhaps more relevant characteristic of these compounds is their low pKa (~3.5) which indicates that the molecules will largely exist in the ionized form (~99.98%). Unlike neutral molecules, the diffusive flux of charged molecules is driven by both entropic factors (i.e. concentration gradient) and enthalpic factors via the electrical potential (i.e. membrane voltage). This membrane voltage, which is maintained by ion channels and transporters in virtually all eukaryotic cells, confers a relative negative voltage to the cell interior as well as the interior of various organelles. As such, this aspect of cell physiology could conceivably contribute to the observed pancreatic and muscle exclusion of carboxylic acids that exist almost exclusively in the anionic form at physiological pH. Conversely, the electrophoretically-driven concentrative uptake of cations, has been extensively applied to the imaging of tumor cells, therapeutic targeting to tumor mitochondria (Modica-Napolitano and Singh, 2002; Hickey *et al.*, 2008) and even the measurement of membrane potential (Hockings and Rogers, 1996).

In this work, we have characterized the pH-dependent permeability of PF-049 and PF-051 in a variety of standard *in vitro* cell systems using a mathematical model of cellular distribution similar to that previously reported for the prediction of tumor cell accumulation of lipophilic bases (Trapp and Horobin, 2005). The model accounts for ionization (according to Henderson-Hasselbalch), passive permeation of neutral molecules (according to Fick's law) and passive permeation of ionized molecules across polarized cell membranes (according to the Nernst-Planck equation). The model also accounts for the physiological values relevant to the cell systems employed in this work. The resulting analysis provides a first-principles explanation for the *in vivo* distributional impairment that is observed not only with regards to the pancreas but also with regards to muscle.

DMD Fast Forward. Published on July 14, 2014 as DOI: 10.1124/dmd.114.058032
This article has not been copyedited and formatted. The final version may differ from this version.

Materials and Methods

Reagents

The hepatoselective glucokinase activators (S)-6-(3-Cyclopentyl-2-(4-(trifluoromethyl)-1H-imidazol-1-yl) propanamido) nicotinic acid (PF-049) (Pfefferkorn *et al.*, 2012) and 6-[(2S)-2-(4-(cyclobutanesulfonyl)-1H-imidazol-1-yl)-3-cyclopentylpropanamido) pyridine-3-carboxylic acid (PF-051) (Stevens *et al.*, 2013) (Figure 1) were used for all the experimental work listed below.

Experimental evaluation of pH-dependent distribution in wild-type and OATP-transfected HEK-293 cells

HEK-293, HEK-293/OATP1B1, and HEK-293/OATP1B3 cells were seeded at a density of 5.6×10^5 cells per well on 48-well poly-D-lysine coated plates and cultured for 72 hours. For the uptake assay, the cells were washed three times with uptake buffer at 37 °C (Hank's Balanced Salt Solution with 20 mM HEPES, pH 7.4) and allowed to equilibrate to uptake buffer at either pH 6.0 or 7.4 for 15 min. After the equilibration period, buffer was discarded and the cells were incubated for 5 min with 200 µL uptake buffer at either pH 6.0 or 7.4 containing 1 µM compound on a heated plate shaker set to 37 °C and 150 rpm. The assay was run at pH 6.0 and 7.4 allowing one to maintain cell viability while varying the ionization fraction of the compound in the media. Cellular uptake was terminated by quickly washing the cells four times on ice with 200 µL ice-cold uptake buffer. The cells were then lysed with 200 µL of a proprietary internal standard (M.W. 686) solution in methanol, and the lysate was injected onto an LC-MS/MS system. The total cellular protein content was determined by using a Pierce bicinchoninic acid (BCA) Protein Assay kit according to the manufacturer's specifications. Model equations for the intracellular uptake of the compound are described by eqn. (5). The relevant physiological parameters for Human Embryonic Kidney 293 (HEK-293) cells are given in Table 1.

Bioanalysis

LC-MS/MS analysis was conducted on a Sciex Triple Quad 4000 mass spectrometer (turbospray ionization source) with a Shimadzu LC-10 HPLC system and Gilson 215 autosampler. The mass spectrometer was controlled by Analyst 1.4.2 software. The LC method consisted of a step gradient with 25 µL samples loaded onto a 1.5×5 mm Showadenko ODP 13 µm particle size column using 95% ammonium acetate buffer (2 mM), 2.5% methanol and 2.5% acetonitrile. Samples were eluted with 10%

DMD Fast Forward. Published on July 14, 2014 as DOI: 10.1124/dmd.114.058032
This article has not been copyedited and formatted. The final version may differ from this version.

ammonium acetate buffer (2 mM), 45% methanol and 45% acetonitrile. The detection was in positive mode with monitored transitions: $397.1 \rightarrow 261.1$ (PF-049), $447.2 \rightarrow 261.3$ (PF-051), $472.3 \rightarrow 436.2$ (Terfenadine, Internal Standard) and $687.0 \rightarrow 320$ (CP-628374, Internal Standard). Peak area counts of analyte compound and internal standard were integrated using DiscoveryQuant Analyze as an add-on to Analyst 1.4.2.

Mathematical model of drug distribution into wild-type and OATP-transfected HEK-293 cells

A model similar to that published previously by Trapp and Horobin is used to characterize the distribution of PF-049 and PF-051 in wild-type and OATP-transfected HEK-293 cells (Trapp and Horobin, 2005; Trapp *et al.*, 2008). Key components of the model are illustrated in Figure 3. The physiological parameters for HEK-293 cells are taken from the literature (Søgaard *et al.*, 2001; Sahni *et al.*, 2012) (Table 1). The associated mathematics are described below. Although the model is applied to acidic molecules, the derived equations are described both for monoprotic acids and bases to facilitate more generalized application.

The Henderson-Hasselbalch relationship is used to calculate the concentration of the ionized and neutral species based on total concentration, pKa of the molecules, and compartmental pH. Eqns. (1) and (2) describe this calculation for acids and bases, respectively:

$$[A^-] = C\frac{10^{pH}}{10^{pH}+10^{pKa}} \qquad [HA] = C\frac{10^{pKa}}{10^{pH}+10^{pKa}} \tag{1}$$

$$[BH^+] = C\frac{10^{pKa}}{10^{pH}+10^{pKa}} \qquad [B] = C\frac{10^{pH}}{10^{pH}+10^{pKa}} \tag{2}$$

where C is the total concentration of the drug molecule, $[A^-]$ and $[BH^+]$ are the concentrations of the ionized species of the acid and base, and finally $[HA]$ and $[B]$ are the concentrations of the neutral species of the acid and base, respectively.

Flux across each membrane and equilibrium distributions are estimated using the previously described Fick's Nernst-Planck framework for compounds that are highly ionized (i.e. compounds with pKa's significantly different from physiological pH) (Ghosh *et al.*, 2014). In this relationship, permeation of the ionized charge can contribute to the total flux even if the ionic permeability is (as expected) much

DMD Fast Forward. Published on July 14, 2014 as DOI: 10.1124/dmd.114.058032
This article has not been copyedited and formatted. The final version may differ from this version.

smaller than the permeability of the neutral species. The flux equations across a single membrane corresponding to acids and bases are as follows:

$$J_{acid} = P_n \cdot SA \cdot \left([HA_0] - [HA_1] \right) - P \cdot SA \cdot \frac{z\Delta\phi F}{RT} \frac{\left([A_1^-] e^{\frac{z\Delta\phi F}{RT}} - [A_0^-] \right)}{e^{\frac{z\Delta\phi F}{RT}} - 1} \quad (3)$$

$$J_{base} = P_n \cdot SA \cdot \left([B_0] - [B_1] \right) - P \cdot SA \cdot \frac{z\Delta\phi F}{RT} \frac{\left([BH_1^+] e^{\frac{z\Delta\phi F}{RT}} - [BH_0^+] \right)}{e^{\frac{z\Delta\phi F}{RT}} - 1} \quad (4)$$

where $[HA_0]$ and $[HA_1]$ ($[B_0]$ and $[B_1]$) are the neutral concentrations of an acid (base) on either side of the membrane, $[A_0^-]$ and $[A_1^-]$ ($[BH_0^+]$ and $[BH_1^+]$) are the ionized concentrations of the acid (base) on either side of the membrane, z is the charge of drug molecule, F is Faraday's constant, $\Delta\phi$ is the electric potential across the membrane, RT is the product of the gas constant and absolute temperature and SA is the relevant surface area. Finally, P_n and P are the permeability constants of the neutral and ionized species respectively. Accounting for cell volumes and intracellular binding, eqns. (1) and (3) can be used to model the kinetics of unbound acidic drugs (e.g. PF-049 and PF-051):

DMD Fast Forward. Published on July 14, 2014 as DOI: 10.1124/dmd.114.058032
This article has not been copyedited and formatted. The final version may differ from this version.

$$
\begin{aligned}
V_{buffer}\frac{dC_{media}}{dt} &= -P_n \cdot SA_{plasma} \cdot \left(C_{media}\frac{10^{pKa}}{10^{pH_{media}}+10^{pKa}} - C_{cell}\frac{fu\cdot 10^{pKa}}{10^{pH_r}+10^{pKa}} \right) \\
&\quad + P \cdot SA_{plasma} \cdot \frac{z\Delta\phi_{plasma}F}{RT} \frac{\left(C_{cell}\frac{fu\cdot 10^{pH_{cell}}}{10^{pH_{cell}}+10^{pKa}} e^{\frac{z\Delta\phi_{plasma}F}{RT}} - C_{media}\frac{10^{pH_{media}}}{10^{pH_{media}}+10^{pKa}} \right)}{e^{\frac{z\Delta\phi_{plasma}F}{RT}}-1} \\
&\quad - Cl_{uptake}\cdot C_{media} \\
V_{cytosol}\frac{dC_{cytosol}}{dt} &= P_n \cdot SA_{plasma} \cdot \left(C_{media}\frac{10^{pKa}}{10^{pH_{media}}+10^{pKa}} - C_{cytosol}\frac{fu\cdot 10^{pKa}}{10^{pH_{cytosol}}+10^{pKa}} \right) \\
&\quad - P \cdot SA_{plasma} \cdot \frac{z\Delta\phi_{plasma}F}{RT} \cdot \frac{\left(C_{cell}\frac{fu\cdot 10^{pH_{cytosol}}}{10^{pH_{cytosol}}+10^{pKa}} e^{\frac{z\Delta\phi_{plasma}F}{RT}} - C_{media}\frac{10^{pH_{media}}}{10^{pH_{media}}+10^{pKa}} \right)}{e^{\frac{z\Delta\phi_{plasma}F}{RT}}-1} \\
&\quad + Cl_{uptake}\cdot C_{media} \\
&\quad - \sum_{organelles} \left(\begin{array}{l} -P_n \cdot SA_{organelle} \cdot \left(fu\cdot C_{cytosol}\frac{10^{pKa}}{10^{pH_{cytosol}}+10^{pKa}} - C_{organelle}\frac{fu\cdot 10^{pKa}}{10^{pH_{organelle}}+10^{pKa}} \right) \\ + P \cdot SA_{organelle} \cdot \frac{z\Delta\phi_{organelle}F}{RT} \frac{\left(C_{cell}\frac{fu\cdot 10^{pH_{organelle}}}{10^{pH_{organelle}}+10^{pKa}} e^{\frac{z\Delta\phi_{organelle}F}{RT}} - C_{cytosol}\frac{10^{pH_{cytosol}}}{10^{pH_{cytosol}}+10^{pKa}} \right)}{e^{\frac{z\Delta\phi_{organelle}F}{RT}}-1} \end{array} \right) \\
V_{organelle}\frac{dC_{organelle}}{dt} &= P_n \cdot SA_{organelle} \cdot \left(fu\cdot C_{cytosol}\frac{10^{pKa}}{10^{pH_{cytosol}}+10^{pKa}} - C_{organelle}\frac{fu\cdot 10^{pKa}}{10^{pH_{organelle}}+10^{pKa}} \right) \\
&\quad - P \cdot SA_{organelle} \cdot \frac{z\Delta\phi_{organelle}F}{RT} \frac{\left(C_{cell}\frac{fu\cdot 10^{pH_{organelle}}}{10^{pH_{organelle}}+10^{pKa}} e^{\frac{z\Delta\phi_{organelle}F}{RT}} - C_{cytosol}\frac{10^{pH_{cytosol}}}{10^{pH_{cytosol}}+10^{pKa}} \right)}{e^{\frac{z\Delta\phi_{organelle}F}{RT}}-1}.
\end{aligned}
\tag{5}
$$

Correspondingly, eqns. (2) and (4) can be used to derive a similar expression for simple bases. The parameters SA_{plasma} and $SA_{organelle}$ are the exposed surface area of the plasma membrane and estimated surface areas of the organelles, fu is the unbound fraction of the drug within the cell, Cl_{uptake} is the active uptake component of the OATP1B1, OATP1B3 transfected cells, and V_{buffer}, $V_{cytosol}$, and $V_{organelle}$ are the volume of the buffer, the cytosolic volume, and the organelle volumes respectively. Estimated volumes of single organelles from the literature for HEK-293 are found in Table 1 and are used to estimate the number of such organelles within the cell type of interest. In turn, this allows one to estimate the total surface area for each organelle type under the simplifying spherical symmetry assumption for all organelles except for

DMD Fast Forward. Published on July 14, 2014 as DOI: 10.1124/dmd.114.058032
This article has not been copyedited and formatted. The final version may differ from this version.

mitochondria for which an ellipsoidal symmetry assumption was used. Note that in this simplified picture, the *fu* is taken to be organelle independent and is instead just a general property of the cell systems. The organelle volumes and surface areas for HEK-293 cells are estimated from the literature and listed in Table 1. The uptake experiments in wild-type (WT), OATP1B1 transfected cells, and OATP1B3 transfected cells were taken out to 5 minutes with samples measuring total intracellular concentration taken in triplicate at 0.5, 1, 1.5, 2, and 5 minutes at both pH 6.0 and 7.4. For each compound, all experimental data points are loaded into Mathematica (Wolfram Research, Inc. Version 9.0.1, Champaign, IL 2013) and fit simultaneously seeking a single unique set of parameters for $P, P_n, Cl_{uptake,1b1,6.0}, Cl_{uptake,1b1,7.4}\ Cl_{uptake,1b3,6.0}, Cl_{uptake,1b3,7.4}$, and fu using the NonlinearModelFit procedure combined with the numerical global optimization algorithm NMinimize using the default settings.

Experimental Determination of Transwell Permeability in MDCK-LE cells

The cell culturing conditions for the in-house low-efflux transporters MDCK (MDCK-LE) cell line (cells isolated from Madin-Darby Canine Kidney cells, selected for low endogenous efflux transporter expression levels) are discussed in more detail elsewhere (Di et al., 2011; Varma et al., 2012). Briefly, MDCK-LE cells were cultured at 37°C, 5% CO_2, 95% relative humidity in minimum essential medium that contained 10% FBS, 1% NEAA, 100U/mL penicillin, 100μg/mL streptomycin and 1% L-glutamine. Cells are passaged each week at about 90% confluency. Cells are then trypsinized and resuspended in complete media to obtain a cell suspension of 2.5×10^5 cells/mL, and then plated onto 96-well membrane inserts, with each insert receiving a volume of 75 μL. Plates were used on day four for transport studies. Cell inserts are washed with pre-warmed ($37°C$) transport buffer before the experiment. Mono-directional transport studies were performed with 2 μM drug solution in transport buffer with 0.1% DMSO. Drug solution was added to the donor wells and buffer was added to the receiver wells to initiate the transport assay. The plates were incubated at 37°C and samples from both the donor and receiver were taken at time 0 min and 90 min for analysis. Permeability of Nadolol, a low permeability marker, was measured to assess the cell monolayer integrity. Trans-epithelial electrical resistance (TEER) values were measured across the cell membranes prior to beginning the experimentation and at the last sample collection time point to assess the integrity of the MDCK-LE monolayers (TEER > 250 Ω cm^2). Permeability was determined at donor pH 5.5, 6.5, and 7.4, with receiver medium pH always 7.4.

DMD Fast Forward. Published on July 14, 2014 as DOI: 10.1124/dmd.114.058032
This article has not been copyedited and formatted. The final version may differ from this version.

Model-based predictions of transcellular permeability in MDCK-LE

The underlying physiochemical transport and uptake processes involved in the MDCK-LE Transwell permeability measurement are shown in Figure 4. A few key simplifying assumptions will be made to derive a tractable model in line with the experimental protocols described in the previous section. As described above, paracellular leakage of MDCK-LE cells was monitored using Nadolol. As such, permeation from the donor to the receiver compartment is expected to occur purely through transcellular passive permeation across the Transwell cellular layer. Additionally, the unstirred water layer (UWL) effect for these compounds is negligible as the permeability of these compounds are well below the aqueous diffusion depletion limit (Ghosh *et al.*, 2014).

Steady state flux conditions are expected to occur when the flux J_{in} across the apical side of the T Transwell layer equals the flux J_{out} coming out of the basolateral side: $J_{in} = J_{out} = J$. Under such steady state flux conditions, uptake into organelles and nonspecific binding no longer contributes to the flux. Using eqn. (3) to represent the flux across each membrane and taking advantage of the fact that the sign on the membrane potential $\Delta\phi$ across the donor-side plasma membrane is equal and opposite to the membrane potential $\Delta\phi$ across the receiver side, J_{in} and J_{out} can be derived as follows:

$$J_{acid,in} = P_n \cdot SA \cdot \left([HA_D] - [HA_i]\right) - P \cdot SA \cdot \frac{z\Delta\phi F}{RT} \frac{\left([A_i^-]e^{\frac{z\Delta\phi F}{RT}} - [A_D^-]\right)}{e^{\frac{z\Delta\phi F}{RT}} - 1}$$
$$J_{acid,out} = P_n \cdot SA \cdot \left([HA_i] - [HA_R]\right) - P \cdot SA \cdot \frac{z\Delta\phi F}{RT} \frac{\left([A_R^-]e^{-\frac{z\Delta\phi F}{RT}} - [A_i^-]\right)}{e^{-\frac{z\Delta\phi F}{RT}} - 1} \quad (6)$$

where the subscripts D, i, and R represent the donor, intracellular, and receiver compartments respectively. Substituting in our Henderson-Hasselbalch relationship (eqn. (1)) yields:

$$J_{acid,in} = P_n \cdot SA \cdot \left(C_D \frac{10^{pKa}}{10^{pH_D} + 10^{pKa}} - C_i \frac{10^{pKa}}{10^{pH_i} + 10^{pKa}} \right) -$$
$$P \cdot SA \cdot \frac{z\Delta\phi F}{RT} \frac{\left(C_i \frac{10^{pH_i}}{10^{pH_i} + 10^{pKa}} e^{\frac{z\Delta\phi F}{RT}} - C_D \frac{10^{pH_D}}{10^{pH_D} + 10^{pKa}} \right)}{e^{\frac{z\Delta\phi F}{RT}} - 1} \quad (7)$$

DMD Fast Forward. Published on July 14, 2014 as DOI: 10.1124/dmd.114.058032
This article has not been copyedited and formatted. The final version may differ from this version.

$$J_{acid,out} = P_n \cdot SA \cdot \left(C_i \frac{10^{pKa}}{10^{pH_i} + 10^{pKa}} - C_R \frac{10^{pKa}}{10^{pH_R} + 10^{pKa}} \right) - P \cdot SA \cdot \frac{z\Delta\phi F}{RT} \frac{\left(C_R \frac{10^{pH_R}}{10^{pH_R} + 10^{pKa}} e^{-\frac{z\Delta\phi F}{RT}} - C_i \frac{10^{pH_i}}{10^{pH_i} + 10^{pKa}} \right)}{e^{-\frac{z\Delta\phi F}{RT}} - 1} \quad (8)$$

Under steady state conditions, $J_{acid,in} = J_{acid,out} = J$, yielding a system of two equations (eqns. (7) and (8)) and two unknowns (J_{acid} and the free intracellular drug concentration C_i). This allows one to solve for the flux J_{acid} as a function of the two measurable quantities (C_D and C_R):

$$J_{acid} = \frac{C_D \left(10^{\mathrm{pH}_R} + 10^{\mathrm{pKa}}\right) \left(\frac{z\Delta\phi F}{RT} P \cdot SA \cdot 10^{\mathrm{pH}_D} + \left(e^{\frac{z\Delta\phi F}{RT}} - 1 \right) 10^{\mathrm{pKa}} P_n \cdot SA \right)}{2 \left(e^{\frac{z\Delta\phi F}{RT}} - 1 \right) \left(10^{\mathrm{pH}_D} + 10^{\mathrm{pKa}}\right) \left(10^{\mathrm{pH}_R} + 10^{\mathrm{pKa}}\right)} - \frac{C_R \left(10^{\mathrm{pH}_D} + 10^{\mathrm{pKa}}\right) \left(\left(e^{\frac{z\Delta\phi F}{RT}} - 1 \right) 10^{\mathrm{pKa}} P_n \cdot SA + \frac{z\Delta\phi F}{RT} P \cdot SA \cdot 10^{\mathrm{pH}_R} \right)}{2 \left(e^{\frac{z\Delta\phi F}{RT}} - 1 \right) \left(10^{\mathrm{pH}_D} + 10^{\mathrm{pKa}}\right) \left(10^{\mathrm{pH}_R} + 10^{\mathrm{pKa}}\right)} \quad (9)$$

which under sink conditions $\left(C_R \to 0\right)$ can be simplified to:

$$\begin{aligned} J_{acid} &= \frac{C_D \left(\frac{z\Delta\phi F}{RT} P \cdot SA \cdot 10^{\mathrm{pH}_D} + \left(e^{\frac{z\Delta\phi F}{RT}} - 1 \right) 10^{\mathrm{pKa}} P_n \cdot SA \right)}{2 \left(e^{\frac{z\Delta\phi F}{RT}} - 1 \right) \left(10^{\mathrm{pH}_D} + 10^{\mathrm{pKa}}\right)} \\ &= \underbrace{\frac{\left(\frac{z\Delta\phi F}{RT} P 10^{\mathrm{pH}_D} + \left(e^{\frac{z\Delta\phi F}{RT}} - 1 \right) 10^{\mathrm{pKa}} P_n \right)}{2 \left(e^{\frac{z\Delta\phi F}{RT}} - 1 \right) \left(10^{\mathrm{pH}_D} + 10^{\mathrm{pKa}}\right)}}_{P_{app}} \cdot SA \cdot C_D \\ &= P_{app} \cdot SA \cdot C_D \end{aligned} \quad (10)$$

Using eqns. (2) and (4), a similar analysis for bases in the Transwell assay, yields the following expression for the flux:

DMD Fast Forward. Published on July 14, 2014 as DOI: 10.1124/dmd.114.058032
This article has not been copyedited and formatted. The final version may differ from this version.

$$J_{base} = \frac{C_D\left(10^{\mathrm{pH}_R}+10^{\mathrm{pKa}}\right)\left(\left(e^{\frac{z\Delta\phi F}{RT}}-1\right)10^{\mathrm{pH}_D}P_n\cdot SA+\frac{z\Delta\phi F}{RT}P\cdot SA\cdot 10^{\mathrm{pKa}}\right)}{2\left(e^{\frac{z\Delta\phi F}{RT}}-1\right)\left(10^{\mathrm{pH}_D}+10^{\mathrm{pKa}}\right)\left(10^{\mathrm{pH}_R}+10^{\mathrm{pKa}}\right)} - \frac{C_R\left(10^{\mathrm{pH}_D}+10^{\mathrm{pKa}}\right)\left(\left(e^{\frac{z\Delta\phi F}{RT}}-1\right)P_n\cdot SA\cdot 10^{\mathrm{pH}_R}+\frac{z\Delta\phi F}{RT}P\cdot SA\cdot 10^{\mathrm{pKa}}\right)}{2\left(e^{\frac{z\Delta\phi F}{RT}}-1\right)\left(10^{\mathrm{pH}_D}+10^{\mathrm{pKa}}\right)\left(10^{\mathrm{pH}_R}+10^{\mathrm{pKa}}\right)} \tag{11}$$

which under sink conditions becomes:

$$\begin{aligned} J_{base} &= \frac{C_D\left(\left(e^{\frac{z\Delta\phi F}{RT}}-1\right)10^{\mathrm{pH}_D}P_n\cdot SA+\frac{z\Delta\phi F}{RT}P\cdot SA\cdot 10^{\mathrm{pKa}}\right)}{2\left(e^{\frac{z\Delta\phi F}{RT}}-1\right)\left(10^{\mathrm{pH}_D}+10^{\mathrm{pKa}}\right)} \\ &= C_D\underbrace{\frac{\left(\left(e^{\frac{z\Delta\phi F}{RT}}-1\right)10^{\mathrm{pH}_D}P_n+\frac{z\Delta\phi F}{RT}P\cdot 10^{\mathrm{pKa}}\right)}{2\left(e^{\frac{z\Delta\phi F}{RT}}-1\right)\left(10^{\mathrm{pH}_D}+10^{\mathrm{pKa}}\right)}}_{P_{app}}\cdot SA \\ &= P_{app}\cdot SA\cdot C_D \end{aligned} \tag{12}$$

We note that under these conditions, the flux term J takes the familiar form of classic 1st order observational passive permeability, but P_{app} is a complex expression of neutral permeability P_n, ionized permeability P, the pKa, and the appropriate electrochemical constants:

$$\begin{aligned} P_{app,acid} &= \frac{\left(\frac{z\Delta\phi F}{RT}P10^{\mathrm{pH}_d}+\left(e^{\frac{z\Delta\phi F}{RT}}-1\right)10^{\mathrm{pKa}}P_n\right)}{2\left(e^{\frac{z\Delta\phi F}{RT}}-1\right)\left(10^{\mathrm{pH}_d}+10^{\mathrm{pKa}}\right)} \\ P_{app,base} &= \frac{\left(\left(e^{\frac{z\Delta\phi F}{RT}}-1\right)10^{\mathrm{pH}_d}P_n+\frac{z\Delta\phi F}{RT}P\cdot 10^{\mathrm{pKa}}\right)}{2\left(e^{\frac{z\Delta\phi F}{RT}}-1\right)\left(10^{\mathrm{pH}_d}+10^{\mathrm{pKa}}\right)} \end{aligned} \tag{13}$$

Under well-stirred sink conditions for strong acids and bases, eqns. (10) and (12) provide an expression for the relative pH dependent flux across the *in vitro* Transwell assay. In the current analysis, eqn. (10) is used to predict the pH-dependent Transwell permeabilities of both PF-049 and PF-051 in MDCK-LE cells using the estimates for P_n and P obtained from modeling uptake kinetics in HEK-293 cells and the physiological parameters (Simmons, 1984; Ishikawa *et al.*, 1998) listed for MDCK-LE cells in Table 1. This allows one

DMD Fast Forward. Published on July 14, 2014 as DOI: 10.1124/dmd.114.058032
This article has not been copyedited and formatted. The final version may differ from this version.

to examine both the translatability of these trans-membrane passive permeability constants across different cell types and the utility of the given mathematical framework.

Quantum Mechanics based Free Energies of Solvation Calculation

Conformational analysis was performed using the OPLS-2005 force field (Jorgensen *et al.*, 1996; Kaminski *et al.*, 2001) with the GB-SA framework (Still *et al.*, 1990). Selected low energy conformations according to OPLS-2005/GB-SA were then energy minimized in water using the B3LYP exchange-correlation energy functional (Becke, 1993; Stephens *et al.*, 1994), the 6-31G* basis set (Frisch *et al.*, 1984) and the Poisson-Boltzmann solver (Tannor *et al.*, 1994) to describe solvent effects. The most stable conformation according to this level of theory was submitted to single-point energy calculations in water at the B3LYP/6-311G**++ level of theory (Marten *et al.*, 1996). All calculations were performed within the Jaguar program (Bochevarov *et al.*, 2013).

Experimental determination of in vivo unbound tissue-to-plasma ratios (Kpuu)

The *in vivo* distribution of PF-049 and PF-051 in male Wistar-Han rat plasma, pancreas, and muscle were determined by measuring unbound tissue concentrations as described previously (Pfefferkorn and Guzman-Perez, 2012; Stevens *et al.*, 2013). PF-049 was dosed at 0.13 mg/mL in PBS (pH 7.4) and PF-051 was dosed at 1.21 mg/mL in 12% (w/v) sulfobutyl ether beta-cyclodextrin acidified with 0.1N HCl. Both drugs were administered through a jugular vein catheter using a flow rate of 4 uL/min (total dose volume 23.04 mL) for 4 days. Plasma, pancreas, and quadriceps muscle were collected from animals under anesthesia and flash frozen for storage until analysis. Drug concentrations were determined by LC-MS/MS analysis of methanol extracts of tissue homogenates. Tissue protein binding was determined in untreated tissue homogenates using equilibrium dialysis. Measured *in vivo Kpuu* are expressed as the ratio of unbound drug in tissue relative to unbound drug in plasma.

Model-based predictions of in vivo tissue-to-plasma ratios

Equilibrium calculations of unbound partition ratios (*Kpuu*) can be derived from the appropriate steady state conditions. For acids, setting eqn. (7) to 0 and solving for the ratio $C_i / C_D = Kpuu^{acid}_{plasma,cytosol}$ yields the following expression for the unbound plasma to cytosol ratio:

DMD Fast Forward. Published on July 14, 2014 as DOI: 10.1124/dmd.114.058032
This article has not been copyedited and formatted. The final version may differ from this version.

$$Kpuu_{plasma,cytosol}^{acid} = \frac{\left(10^{pH_r} + 10^{pKa}\right)\left(\frac{z\Delta\phi F}{RT} P10^{pH_d} + \left(e^{\frac{z\Delta\phi F}{RT}} - 1\right)10^{pKa} P_n\right)}{\left(10^{pH_d} + 10^{pKa}\right)\left(\left(e^{\frac{z\Delta\phi F}{RT}} - 1\right)10^{pKa} P_n + e^{\frac{z\Delta\phi F}{RT}} \frac{z\Delta\phi F}{RT} P10^{pH_r}\right)} \quad (14)$$

and correspondingly a similar relationship for bases can be derived yielding:

$$Kpuu_{plasma,cytosol}^{base} = \frac{\left(10^{pH_r} + 10^{pKa}\right)\left(\left(e^{\frac{z\Delta\phi F}{RT}} - 1\right)10^{pH_d} P_n + \frac{z\Delta\phi F}{RT} P10^{pKa}\right)}{\left(10^{pH_d} + 10^{pKa}\right)\left(\left(e^{\frac{z\Delta\phi F}{RT}} - 1\right) P_n 10^{pH_r} + e^{\frac{z\Delta\phi F}{RT}} \frac{z\Delta\phi F}{RT} P10^{pKa}\right)} \quad (15)$$

For organelles within a cell, it can be easily shown that the equilibrium partitioning must be multiplicative in nature:

$$Kpuu_{plasma,organelle} = Kpuu_{plasma,cytosol} \times Kpuu_{cytosol,organelle} \quad (16)$$

Correspondingly, the unbound partitioning between the cytosol and any organelle are also described by eqns. (14) or (15) where the donor compartment is now the cytosol and the receiver compartment is now the organelle in question. Note that the equilibrium partition coefficients *Kpuu* are *independent* of organelle or cell volume. As with the purely prospective predictions of the MDCK-LE observed permeabilities, eqn. (16) is also used purely prospectively to predict *in vivo Kpuu* using the permeability parameters derived from the transfected HEK-293 assay.

The relevant parameters (voltage, pH and fractional volume) for estimating the unbound partitioning within muscle (Guderley *et al.*, 2006; Sawant *et al.*, 2011) , liver (Peters, 1984; Saito *et al.*, 1992; Plettenberg *et al.*, 2008) and the pancreas (Nishiyama and Petersen, 1974; Morgan *et al.*, 1986; Taga *et al.*, 1993) are provided in Table 1. The key approximation that will be made within this framework is that the trans-membrane permeation is similar across various cell and organelle types and that *fu* is a whole tissue parameter. As the membrane composition may differ across tissue types this is clearly a simplifying approximation that should be tested more thoroughly.

DMD Fast Forward. Published on July 14, 2014 as DOI: 10.1124/dmd.114.058032
This article has not been copyedited and formatted. The final version may differ from this version.

Results

Characterization of pH dependent distribution in wild-type and OATP-transfected HEK-293 cells

PF-049 and its structural analog, PF-051 were analyzed to determine pH dependent OATP1B1 / OATP1B3 uptake, passive permeability, and fraction unbound within the cell. All relevant parameters were fit simultaneously using eqn. (5) for all cell line (WT, OATP1B1, OATP1B3) data to derive a self-consistent single set of parameters. Kinetic data for PF-049 and PF-051 were reasonably well described by the proposed mathematical model for WT HEK 293 cells at both pH 6.0 and 7.4 (Figures 5 and 6, open symbol / dashed lines). As expected, the estimated passive permeability of the ionized species (P) of each drug molecule is lower than the neutral species (P_n). However, the ratio of these values is much larger for PF-049 (i.e. 357) than for PF-051 (i.e. 4.1). This is consistent with visual inspection of the kinetic data obtained in WT HEK cells, which indicate that cellular accumulation of PF-049 is more sensitive to pH than that of PF-051. The relatively larger P_n of PF-049 manifests as a compound that is balanced between neutral-dominated and ionized permeability profiles where cell uptake is more sensitive to the expected change to unionized fraction (Figure 5, open symbols). In contrast, the relatively lower P_n of PF-051 manifests as a completely ionized-dominated permeability profile where cell uptake is insensitive to the expected change in unionized fraction (Figure 6, open symbols). The potential physicochemical basis for this difference is addressed in the discussion.

Kinetic data for PF-049 and PF-051 were also well described by the proposed mathematical model for OATP 1B1 and 1B3 transfected HEK 293 cells at both pH 6.0 and 7.4 (Figures 5 and 6, closed symbol / solid lines). As expected, accumulation is increased relative to WT HEK 293 cells. Data were best characterized by allowing for a pH-dependent active uptake rate. For example, consistent with what has been previously reported for OATP 2B1-mediated uptake of statins (Varma *et al.*, 2011) , the estimated uptake rate of PF-051 was significantly larger at pH 6.0 relative to pH 7.4 (Table 2). A reverse trend was observed with respect to PF-049, though this did not reach statistical significance. The model-derived uptake rates indicate that PF-049 is transported more rapidly than PF-051 in 1B3 and 1B1-transfected HEK cells, respectively (Table 2). These results suggest that unlike in rats (figure 2), PF-049 may have a human

DMD Fast Forward. Published on July 14, 2014 as DOI: 10.1124/dmd.114.058032
This article has not been copyedited and formatted. The final version may differ from this version.

hepatoselectivity advantage over PF-051, though further investigation would be required to support this possibility.

Prediction of pH dependent transcellular permeability in MDCK-LE cells

Both PF-049 and PF-051 demonstrated pH dependent permeability in MDCK-LE cells (Table 3). As a test of the mathematical framework and translatability of passive permeabilities across cell lines, eqn. (10) was used to predict these results assuming the relevant physiological parameters for MDCK-LE cells listed in Table 2 and values of P_n and P estimated from HEK-293 cells listed in Table 2. These predictions were generally consistent with the overall pH dependent trend and the absolute values determined experimentally (Table 3, predicted vs. observed). As observed with accumulation in WT HEK cells, the experimental and predicted P_{obs} of PF-049 was more sensitive to pH than that for PF-051 (Table 3). This again can be attributed to the fact that PF-049 has a much larger ratio of P_n and P. Given that both compounds have a pKa of 3.5, the fraction unionized is low and proportionally related to the pH across the range of values examined (i.e. pH 7.4, 6.5, 5.5 approximately 0.01, 0.1 and 1 % unionized, respectively). As such, if overall MDCK permeation is predominately determined only by the neutral species, then the apparent permeability should be inversely proportional to pH. Likewise, the fraction ionized is high and relatively independent of pH across the range of values examined (i.e. pH 7.4, 6.5, 5.5 roughly corresponds to 99, 99.9 and 99.99 % ionized, repectively). As such, if the overall MDCK permeation is predominately determined by the ionized species, then the apparent permeability should be independent of pH. The results listed in table 3 are consistent with a contribution of both ionized and unionized fractions to the overall MDCK permeability (i.e. some sensitivity in P_{app} short of a strict inverse proportionality). The relatively greater pH sensitivity of PF-049 (both observed and predicted) is attributed to the fact that it has a neutral permeability which is much greater than the ionized permeability (1868 vs. 5.23 $x10^{-6}$ cm/sec, table 2). In contrast, PF-051 has a much lower neutral permeability relative to the ionized permeability (18.2 vs. 4.43 $x10^{-6}$ cm/sec, table 2), a property which lends itself to being insensitive over the lower range of pHs studied.

Prediction of in vivo unbound tissue-to-plasma ratios in the muscle and pancreas

DMD Fast Forward. Published on July 14, 2014 as DOI: 10.1124/dmd.114.058032
This article has not been copyedited and formatted. The final version may differ from this version.

Consistent with distributional impairment, the experimentally determined steady state *Kpuu* values of both PF-049 and PF-051 in rat muscle and pancreas were significantly lower than 1 (Table 4). This property of pancreatic exclusion contributes further to the pharmacological *selectivity* of these agents for liver GK relative to GK in the pancreas. As stated previously, these results cannot simply be explained by Fick's law as this would require *Kpuu* to equal unity at steady state. As an additional test of the proposed mathematical framework and the hypothesis that this exclusion is driven by membrane potential, eqns. (14) and (16) were used to predict *Kpuu* assuming the relevant physiological pancreatic and muscle parameters listed in Table 1 and the values of P and P_n derived from HEK-293 cells listed in Table 2. As shown in Table 4, model predictions were generally consistent with experimental results for both compounds across both muscle and pancreas.

DMD Fast Forward. Published on July 14, 2014 as DOI: 10.1124/dmd.114.058032
This article has not been copyedited and formatted. The final version may differ from this version.

Discussion

Characterization of passive permeability using pH dependent distribution in wild-type and OATP-transfected HEK-293 cell lines and Analysis

Results obtained by modeling the HEK-293 cell data indicate that the ionized species of PF-049 and PF-051 have similar permeabilities (5.23×10^{-6} cm/s and 4.43×10^{-6} cm/s, respectively). Qualitatively, this is due to the similar structure around the carboxylic acid group that is expected to limit permeability in the ionized state (Figure 1). The two compounds differ by substitution on the imidazole ring. PF-049 has a hydrophobic trifluoromethyl group, while PF-051 has a more hydrophilic cyclobutylsulfone group. For both compounds, the negative charge of the carboxylate group is expected to be a limiting factor for permeation with a modest contribution from the remaining substitutions.

To quantify the physiochemical basis for why the neutral permeabilities for PF-049 and PF-051 are so different from each other, in contrast to the ionized permeabilities, the free energies of solvation were calculated using the SCRF approach. The free energies of solvation are used as a simplified surrogate to estimate the free energies associated with stripping the water molecules upon insertion in the membrane. The negatively charged PF-049 and PF-051 were calculated to have hydration free energies of -79.56 and -86.56 kcal/mol, respectively. The absolute numbers are so negative that the -7 kcal/mol difference between the hydration free energies becomes irrelevant; they both display equally low permeabilities for the ionized state. In the neutral state, PF-049 and PF-051 have less pronounced hydration free energies, -23.60 and -31.19 kcal/mol respectively, again approximately -7.0 kcal/mol favoring the hydration of the cyclobutylsulfone group. For a neutral molecule, the -7.0 kcal/mol extra hydration solvation free energy is expected to play a more significant role. We hypothesize that it is this relative hydration penalty between PF-049 and PF-051 that leads to the much lower permeability for the neutral state of PF-051, yet similar permeability for the ionized fractions.

Forward Predictions – MDCK-LE Transwell prediction

For both compounds, predictions employing the permeabilities derived from the HEK-293 cell data are in agreement with that observed in the MDCK-LE Transwell system across 3 different pH's. The translatability in passive permeability parameters between HEK-293 cells and MDCK-LE cells is at odds with recent speculation that passive permeation is a transporter mediated phenomenon (Dobson and Kell,

DMD Fast Forward. Published on July 14, 2014 as DOI: 10.1124/dmd.114.058032
This article has not been copyedited and formatted. The final version may differ from this version.

2008; Kell *et al.*, 2011). With regards to the mathematical model, we note that although observed permeability (P_{obs}) collapses into its more phenomenological form $\left(J \approx P_{obs}\left(C_o - C_i\right)\right)$, the term P_{obs} is itself a complex formula of physiochemical parameters: neutral passive permeability P_n, ionized passive permeability P, the pKa of the compound, and physiological parameters: the underlying membrane potential of the cell ϕ and local pH. An examination of eqn. (13) provides a possible hypothesis for the observation that acids tend to be less permeable than bases (Palm *et al.*, 1999; Clark, 2003; Lobell *et al.*, 2003; Fridén *et al.*, 2009) based on the physiochemical properties of the drug and the physiology of the cell. To illustrate, we take two hypothetical molecules: one acid and one base both of which are assumed to have the P_n and P values estimated for PF-049 (i.e. 1868 and 5.23×10^{-6} cm/sec). Using eqn. (13), we have calculated expected Transwell permeabilities for both molecules as a function of *pKa* under conditions of physiological pH (i.e. pH=7.4). Figure 7 illustrates the Transwell permeability calculated as a function of *pKa* for an acid (in red) and base (in blue). It is clear that acids and bases do not exhibit the same symmetry when ionized even if the physiochemical permeability properties of the neutral and ionized permeabilities are the same. The observed Transwell permeability rates of charged acids (at low *pKa*) are much lower than the observed Transwell permeability rates of charged bases (at high *pKa*) even though the intrinsic permeability constants of the two compounds are exactly the same (Figure 7). At steady state flux conditions (eqn. (13)), the membrane potential acts as an additional barrier for strong acids, decreasing the flux into the receiver compartment. Conversely, the membrane potential can serve to increase the intracellular drug concentration for strong bases, increasing the flux into the receiver compartment. This may provide another explanation for common observations that the physiochemical properties of compounds that are known to traverse the blood brain barrier tend to be relatively lipophilic basic compounds rather than acidic compounds. Further, this may provide another basis underlying the design strategy of using the physiochemical properties of lipophilic cations for central nervous system penetration (Tamai *et al.*, 1997; Tsuji, 2005; Ribeiro *et al.*, 2012).

Forward Predictions – in vivo Kpuu

The concordance between model predictions and *in vivo* data suggests that the distribution of both PF-049 and PF-051 at physiological pH occurs predominately through the anionic fraction, a property that

DMD Fast Forward. Published on July 14, 2014 as DOI: 10.1124/dmd.114.058032
This article has not been copyedited and formatted. The final version may differ from this version.

confers a voltage-driven distributional exclusion according to the Nernst-Planck relationship. It is somewhat unintuitive why this should occur even when the permeability of the ionized species can be orders of magnitude lower than the neutral form. The lower permeability of ionized forms often leads to distributional behaviors that are much more in line with Fick's law and pH partitioning (Shore *et al.*, 1957; Schanker, 1962; Friden *et al.*, 2011; Avdeef, 2012). An examination of the determinants for total flux allows one to understand the circumstances that lead to these two extremes. Rewriting eqn. (3) in its simplest form below, we see that the total flux of acids is approximately proportional to the permeabilities of each species multiplied by its concentration:

$$J \propto P_n[HA] + P[A^-] \tag{17}$$

An acid will follow a Nernst-Planck distribution only when the product of P and $[A^-]$ exceeds that of the product of P_n and $[HA]$. Both PF-049 and PF-051 have pKa values of 3.5. The 6300-fold ratio of ionized to neutral species at physiological pH is expected to completely offset the observed P_n to P ratios for PF-049 and PF-051 (i.e. 357 and 4 respectively). In such cases, the enthalpic contribution from the membrane potential (eqn. (14) and eqn. (15)) will govern the equilibrium partitioning of the drug and lead to a degree of intracellular exclusion. Conversely, if the product of $P_n[HA]$ exceeds that of $P[A^-]$, these equations collapse back to the classical pH partitioning equations, the underlying mechanism that governs for instance cationic accumulation of drugs within lysosomes (Kaufmann and Krise, 2007; Friden *et al.*, 2011). In this sense, the derived equilibrium equations for steady state partitioning (*Kpuu*) (eqns. (14) and (15)) should be considered as simply an organelle specific generalization of classical pH partitioning behavior.

Fick's law and classical pH partitioning hold for weak acids and weak bases with a characteristic localized charge in the ionized form that renders the ionized species impermeable to a hydrophobic barrier. However, in cases where charge delocalization yields a lipophilic acid (or base) or the *pKa* of the drug is such that the abundance of the charged species is many orders of magnitude higher than its neutral counterpart, the enthalpic contribution of membrane potential must be considered. Using these basic physiochemical properties, we are able to design glucokinase agonists with a greater therapeutic index of the compound than simply taking a pure transporter driven hepatoselective uptake approach (Figure 2). This approach not only maximizes the known therapeutic index (TI), minimizing hypoglycemic risk due to

DMD Fast Forward. Published on July 14, 2014 as DOI: 10.1124/dmd.114.058032
This article has not been copyedited and formatted. The final version may differ from this version.

insulin stimulation and also has the advantage of minimizing other off-target risk by minimizing exposure to non-target tissues.

As has been shown with our glucokinase agonists, unbound tissue / organelle accumulation or exclusion are driven by a mixture of the physiochemical properties of the drug (P, P_n, pKa) and the physiological properties of the cell and its relevant organelles (membrane potential ϕ, pH). In Figure 8, the predicted $Kpuu_{plasma,cytosol}$ in the pancreas for an acidic compound with a fixed *pKa* of 3.5 as a function of the neutral permeability P_n and the ionized permeability P is shown. In this figure, PF-049 and PF-051 are shown in red and blue respectively, illustrating how for the case of the two clinical candidates, the compounds have a balance of properties which provide for pancreatic exclusion at the target site. It is also clear that there is a large optimum (i.e. low $Kpuu$) space for molecules with *pKa* values in this range. We note that this relationship is only valid for molecules with a *pKa* of 3.5 and that the optimum space becomes increasingly restricted at higher *pKa* values (data not shown).

Conclusions

We have shown that a single set of physiochemical properties of a compound (P, P_n, pKa) can be used to derive a self-consistent parameterization of time-dependent uptake measurement as well as Transwell permeability measurements. Further it has been shown that in combination with a few key physiological parameters, the same set of parameters can be used to derive the equilibrium unbound $Kpuu$ in non-clearing organs through a non-transporter mediated efflux or uptake mechanism. Analytical expressions for the equilibrium $Kpuu$ for tissues and organelles of interest have been derived. We have shown that physiochemical properties of our glucokinase agonist compounds govern exposure in certain organelles and tissues, providing an optimal therapeutic index by minimizing exposure in non-hepatic tissues.

Authorship Contributions

Participated in research design: Ghosh, Scott, Maurer, Gulliermas, Tu, Scialis

Conducted experiments: Rotter, Scialis

Contributed new reagents or analytic tools: Varma, Feng, Scialis

Performed data analysis: Ghosh, Gulliermas, Tu

Wrote or contributed to the writing of the manuscript: Ghosh, Scott, Maurer, Guimaraes, Tu, Varma, Litchfield

DMD Fast Forward. Published on July 14, 2014 as DOI: 10.1124/dmd.114.058032
This article has not been copyedited and formatted. The final version may differ from this version.

References

Avdeef A (2012) *Absorption and Drug Development: Solubility, Permeability, and Charge State*, 2nd ed., John Wiley & Sons.

Becke AD (1993) A new mixing of Hartree–Fock and local density-functional theories. *J Chem Phys* **98**:1372–1377, AIP Publishing.

Bochevarov AD, Harder E, Hughes TF, Greenwood JR, Braden DA, Philipp DM, Rinaldo D, Halls MD, Zhang J, and Friesner RA (2013) Jaguar: A high-performance quantum chemistry software program with strengths in life and materials sciences. *Int J Quantum Chem* **113**:2110–2142.

Clark DE (2003) In silico prediction of blood-brain barrier permeation. *Drug Discov Today* **8**:927–933.

Dobson PD, and Kell DB (2008) Carrier-mediated cellular uptake of pharmaceutical drugs: an exception or the rule? *Nat Rev Drug Discov* **7**:205–220.

Friden M, Bergstrom F, Wan H, Rehngren M, Ahlin G, Hammarlund-Udenaes M, and Bredberg U (2011) Measurement of Unbound Drug Exposure in Brain: Modeling of pH Partitioning Explains Diverging Results between the Brain Slice and Brain Homogenate Methods. *Drug Metabolism and Disposition* **39**:353–362.

Fridén M, Winiwarter S, Jerndal G, Bengtsson O, Wan H, Bredberg U, Hammarlund-Udenaes M, and Antonsson M (2009) Structure-brain exposure relationships in rat and human using a novel data set of unbound drug concentrations in brain interstitial and cerebrospinal fluids. *J Med Chem* **52**:6233–6243.

Frisch MJ, Pople JA, and Binkley JS (1984) Self-consistent molecular orbital methods 25. Supplementary functions for Gaussian basis sets. *J Chem Phys* **80**:3265–3269, AIP Publishing.

Ghosh A, Scott DO, and Maurer TS (2014) Towards a unified model of passive drug permeation I: Origins of the unstirred water layer with applications to ionic permeation. *Eur J Pharm Sci* **52**:109–124.

Golden PL, and Pollack GM (2003) Blood–brain barrier efflux transport. *J Pharm Sci* **92**:1739–1753.

Grimsby J, Sarabu R, Corbett WL, Haynes N-E, Bizzarro FT, Coffey JW, Guertin KR, Hilliard DW, Kester RF, Mahaney PE, Marcus L, Qi L, Spence CL, Tengi J, Magnuson MA, Chu CA, Dvorozniak MT, Matschinsky FM, and Grippo JF (2003) Allosteric activators of glucokinase: potential role in diabetes therapy. *Science* **301**:370–373.

Guderley HH, Houle-Leroy PP, Diffee GMG, Camp DMD, and Garland TT (2006) Morphometry, ultrastructure, myosin isoforms, and metabolic capacities of the "mini muscles“" favoured by selection for high activity in house mice. *Comp Biochem Physiol B Biochem Mol Biol* **144**:12–12.

Hickey JL, Ruhayel RA, Barnard PJ, Baker MV, Berners-Price SJ, and Filipovska A (2008) Mitochondria-Targeted Chemotherapeutics: The Rational Design of Gold(I) N-Heterocyclic Carbene Complexes That Are Selectively Toxic to Cancer Cells and Target Protein Selenols in Preference to Thiols. *J Am Chem Soc* **130**:12570–12571, American Chemical Society.

Hockings PD, and Rogers PJ (1996) The measurement of transmembrane electrical potential with lipophilic

cations. *Biochim Biophys Acta* **1282**:101–106.

Ishikawa T, Marunaka Y, and Rotin D (1998) Electrophysiological characterization of the rat epithelial Na+ channel (rENaC) expressed in MDCK cells. Effects of Na+ and Ca2+. *The Journal of General Physiology* **111**:825–846.

Jorgensen WL, Maxwell DS, and Tirado-Rives J (1996) Development and Testing of the OPLS All-Atom Force Field on Conformational Energetics and Properties of Organic Liquids. *J Am Chem Soc* **118**:11225–11236, American Chemical Society.

Kaminski GA, Friesner RA, Tirado-Rives J, and Jorgensen WL (2001) Evaluation and Reparametrization of the OPLS-AA Force Field for Proteins via Comparison with Accurate Quantum Chemical Calculations on Peptides. *J Phys Chem B* **105**:6474–6487.

Kaufmann AM, and Krise JP (2007) Lysosomal sequestration of amine-containing drugs: analysis and therapeutic implications. *J Pharm Sci* **96**:729–746.

Kell DB, Dobson PD, and Oliver SG (2011) Pharmaceutical drug transport: the issues and the implications that it is essentially carrier-mediated only. *Drug Discov Today* **16**:704–714.

Lobell M, Moln r LS, and Keser GRM (2003) Recent advances in the prediction of blood-brain partitioning from molecular structure. *J Pharm Sci* **92**:360–370.

Marten B, Kim K, Cortis C, Friesner RA, Murphy RB, Ringnalda MN, Sitkoff D, and Honig B (1996) New Model for Calculation of Solvation Free Energies: Correction of Self-Consistent Reaction Field Continuum Dielectric Theory for Short-Range Hydrogen-Bonding Effects. *J Phys Chem* **100**:11775–11788, American Chemical Society.

Matschinsky FM (2009) Assessing the potential of glucokinase activators in diabetes therapy. *Nat Rev Drug Discov* **8**:399–416.

Matschinsky FM (2013) GKAs for diabetes therapy: why no clinically useful drug after two decades of trying? *Trends Pharmacol Sci* **34**:90–99.

Modica-Napolitano JS, and Singh KK (2002) Mitochondria as targets for detection and treatment of cancer. *Expert Rev Mol Med* **4**:1–19.

Morgan RG, Schaeffer BK, and Longnecker DS (1986) Size and number of nuclei differ in normal and neoplastic acinar cells from rat pancreas. *Pancreas* **1**:37–43.

Nishiyama A, and Petersen OH (1974) Pancreatic acinar cells: membrane potential and resistance change evoked by acetylcholine. *J Physiol (Lond)* **238**:145–158.

Palm K, Luthman K, Ros J, Grasjo J, and Artursson P (1999) Effect of molecular charge on intestinal epithelial drug transport: pH-dependent transport of cationic drugs. *J Pharmacol Exp Ther* **291**:435–443.

Peters R (1984) Nucleo-cytoplasmic flux and intracellular mobility in single hepatocytes measured by fluorescence microphotolysis. *EMBO J* **3**:1831–1836.

Pfefferkorn JA, and Guzman-Perez A (2012) Discovery of (S)-6-(3-Cyclopentyl-2-(4-(trifluoromethyl)-1H-imidazol-1-yl)propanamido)nicotinic Acid as a Hepatoselective Glucokinase Activator Clinical Candidate for Treating Type 2 Diabetes Mellitus - Journal of Medicinal Chemistry (ACS Publications). *J Med Chem* **55**:1318–1333.

Pfefferkorn JA, Tu M, Filipski KJ, Guzman-Perez A, Bian J, Aspnes GE, Sammons MF, Song W, Li J-C, Jones CS, Patel L, Rasmusson T, Zeng D, Karki K, Hamilton M, Hank R, Atkinson K, Litchfield J, Aiello R, Baker L, Barucci N, Bourassa P, Bourbounais F, D'Aquila T, Derksen DR, Macdougall M, and Robertson A (2012) The design and synthesis of indazole and pyrazolopyridine based glucokinase activators for the treatment of type 2 diabetes mellitus. *Bioorg Med Chem Lett* **22**:7100–7105.

Plettenberg S, Weiss EC, Lemor R, and Wehner F (2008) Subunits alpha, beta and gamma of the epithelial Na+ channel (ENaC) are functionally related to the hypertonicity-induced cation channel (HICC) in rat hepatocytes. *Pflugers Arch* **455**:1089–1095.

Ribeiro MMB, Domingues MM, Freire JM, Santos NC, and Castanho MARB (2012) Translocating the blood-brain barrier using electrostatics. *Front Cell Neurosci* **6**:1–7.

Sahni M, Wilcox S, Mettner P, Reiss C, gilliland S, Purtle D, and Etchberger KJ (2012) *HEK 293 Cell Growth and Virus Production in EX-CELL® 293 Serum-Free Medium.*

Saito S, Murakami Y, Miyauchi S, and Kamo N (1992) Measurement of plasma membrane potential in isolated rat hepatocytes using the lipophilic cation, tetraphenylphosphonium: correction of probe intracellular binding and mitochondrial accumulation. *Biochim Biophys Acta* **1111**:221–230.

Sawant A, Garland SJ, House AA, and Overend TJ (2011) Morphological, electrophysiological, and metabolic characteristics of skeletal muscle in people with end-stage renal disease: a critical review. *Physiother Can* **63**:355–376.

Schanker LS (1962) Passage of drugs across body membranes. *Pharmacol Rev* **14**:501–530.

Shore PA, Brodie BB, and Hogben CA (1957) The gastric secretion of drugs: a pH partition hypothesis. *J Pharmacol Exp Ther* **119**:361–369.

Simmons NL (1984) Epithelial cell volume regulation in hypotonic fluids: studies using a model tissue culture renal epithelial cell system. *Q J Exp Physiol* **69**:83–95.

Stephens PJ, Devlin FJ, and Chabalowski CF (1994) Ab initio calculation of vibrational absorption and circular dichroism spectra using density functional force fields. *J Phys Chem* **98**:11623–11627.

Stevens BD, Litchfield J, Pfefferkorn JA, Atkinson K, Perreault C, Amor P, Bahnck K, Berliner MA, Calloway J, Carlo A, Derksen DR, Filipski KJ, Gumkowski M, Jassal C, Macdougall M, Murphy B, Nkansah P, Pettersen J, Rotter C, and Zhang Y (2013) Discovery of an intravenous hepatoselective glucokinase activator for the treatment of inpatient hyperglycemia. *Bioorg Med Chem Lett* **23**:6588–6592.

Still WC, Tempczyk A, Hawley RC, and Hendrickson T (1990) Semianalytical treatment of solvation for molecular mechanics and dynamics. *J Am Chem Soc* **112**:6127–6129.

Søgaard R, Ljungstrøm T, Pedersen KA, Olesen SP, and Jensen BS (2001) KCNQ4 channels expressed in mammalian cells: functional characteristics and pharmacology. *American Journal of Physiology-Cell Physiology* **280**:C859–C866.

Taga R, Alvares EP, and Sesso A (1993) Morphometric studies on terminal tubule and acinar cells in developing submandibular gland of the rat. *Arch Histol Cytol* **56**:517–523.

Tamai I, Sai Y, Kobayashi H, Kamata M, Wakamiya T, and Tsuji A (1997) Structure-internalization relationship for adsorptive-mediated endocytosis of basic peptides at the blood-brain barrier. *J Pharmacol Exp Ther* **280**:410–415.

Tannor DJ, Marten B, and Murphy R (1994) Accurate first principles calculation of molecular charge distributions and solvation energies from ab initio quantum mechanics and continuum dielectric theory. *J Am Chem Soc* **116**:11875–11882.

Trapp S, and Horobin RW (2005) A predictive model for the selective accumulation of chemicals in tumor cells. *Eur Biophys J* **34**:959–966.

Trapp S, Rosania GR, Horobin RW, and Kornhuber J (2008) Quantitative modeling of selective lysosomal targeting for drug design. *Eur Biophys J* **37**:1317–1328.

Tsuji A (2005) Small molecular drug transfer across the blood-brain barrier via carrier-mediated transport systems. *Neurotherapeutics* **2**:54–62.

Varma MV, Rotter CJ, Chupka J, Whalen KM, Duignan DB, Feng B, Litchfield J, Goosen TC, and El-kattan AF (2011) pH-sensitive interaction of HMG-CoA reductase inhibitors (statins) with organic anion transporting polypeptide 2B1. *Mol Pharm* **8**:1303–1313.

DMD Fast Forward. Published on July 14, 2014 as DOI: 10.1124/dmd.114.058032
This article has not been copyedited and formatted. The final version may differ from this version.

Figure Legends

Figure 1. Chemical structure of PF-049 and PF051 are shown. Note the similar local structural motif around the carboxylic acid groups (shown in brackets).

Figure 2. Steady-state unbound tissue-to-plasma exposure of PF-049 and PF-051 determined in rats post 4 day infusion. Error bars represents the S.D. in the in vivo unbound tissue/plasma ratios determined within rats (n=3). Unbound exposures were calculated using mean unbound fractions. For PF-051 fu_{plasma}, $fu_{pancreas}$, fu_{liver} and fu_{muscle} were 0.19, 0.17, 0.17 and 0.41 (%CV% $\leq$ 10), respectively. For PF-051 fu_{plasma}, $fu_{pancreas}$, fu_{liver} and fu_{muscle} were 0.096, 0.11, 0.07 and 0.19 (%CV < 16), respectively.

Figure 3. Model structure for unbound tissue distribution across plasma and organelles.

Figure 4. The underlying physiochemical transport and uptake processes involved in the MDCK-LE Transwell permeability measurement under low permeability conditions. Note that under steady state flux conditions, organelles play a similar role as *fu*, dropping out of the final expression (eqn. (13)).

Figure 5. Wild-type (dashed) and transfected 1B1/1B3 uptake (solid) of PF-049 into HEK-293 cells at pH 7.4 and 6.0. Concentrations represent total cell associated PF-049 (bound and free) as modeled.

Figure 6. Wild-type (dashed) and transfected 1B1/1B3 uptake (solid) of PF-051 into HEK-293 cells at pH 7.4 and 6.0. Concentrations represent total cell associated PF-051 (bound and free) as modeled.

Figure 7. Predicted apparent permeability of a hypothetical acid (red) and base (blue) with intrinsic permeabilities $P = 5.23 \times 10^{-6}$ cm/s and $P_n = 1868 \times 10^{-6}$ cm/s as a function of pKa across a MDCK-LE Transwell system at physiological pH (7.4). The observed Transwell permeability is lower for acids in comparison to bases with the same physiochemical properties (P, P_n).

Figure 8. Predicted steady state pancreatic *Kpuu* for the acidic glucokinase agonists PF-049 and PF-51 in pancreatic cells. The plot represents the relationship to P and P_n for an acid with a pKa of 3.5.

DMD Fast Forward. Published on July 14, 2014 as DOI: 10.1124/dmd.114.058032
This article has not been copyedited and formatted. The final version may differ from this version.

Tables

Table 1: Organelle Parameters for various *in vitro* cell lines and tissues

Liver Hepatocyte	cytosol	mitochondria	lysosome	Nucleus
Voltage (mV)	-37.9	-167	18.6	-9.2
pH	7.2	8	4.7	7.2
Volume (%)	62.8	28.3	0.8	
Muscle (mouse) Cardiac	cytosol	mitochondria	nucleus	
Voltage (mV)	-85	-167	-9.2	
pH	6.9	8	7.2	
Volume (%)	8.2	37.5	3.6	
Muscle (guinea pig) soleus (slow oxidative)	cytosol	mitochondria	nucleus	
Voltage (mV)	-69.7	-167	-9.2	
pH	7.12	8	7.2	
Volume (%)	7.36	4.9	3.6	
Muscle (guinea pig) white vastus (fast glycolytic)	cytosol	mitochondria	nucleus	
Voltage (mV)	-85.3	-167	-9.2	
pH	7.12	8	7.2	
Volume (%)	15.94	1.9	3.6	
Muscle (guinea pig) red vastus (fast oxidative)	cytosol	mitochondria	nucleus	
Voltage (mV)	-71.7	-167	-9.2	
pH	7.12	8	7.2	
Volume (%)	15.94	1.9	3.6	
Pancreas (Acinar cells)	cytosol	mitochondria	nucleus	
Voltage (mV)	-40	-167	-9.2	
pH	7.2	8	7.2	
Volume		8	10	
HEK-293 Cells	cytosol	mitochondria	nucleus	
Voltage (mV)	-56	-167	18.6	
pH	7.2	8	4.7	
Volume (%)	35	25	30	
MDCK-LE Cells	cytosol	mitochondria	nucleus	
Voltage (mV)	-47.6	-167	18.6	
pH	7.3	8	4.7	
Volume (%)	70	10	17	

Single Mitochondrial SA: 1.19 $*10^{-7}$ cm^2
Single Mitochondrial Volume: 2.26 fl
(used to estimate number of mitochondria)
Nuclear SA: (est. from fract. vol. and spherical sym.)
Single Lysosomal Volume: 0.5 fl
Single Lysosomal SA: (est. from spherical sym.)

DMD Fast Forward. Published on July 14, 2014 as DOI: 10.1124/dmd.114.058032
This article has not been copyedited and formatted. The final version may differ from this version.

Table 2: Model-derived parameters for passive permeability, fu and active uptake determined in HEK 293 cells

	PF-049		PF-051		Units
p	5.23	(4.06 .. 6.78)	4.43	(3.4 ..5.8)	(x 10^{-6} cm/s)
p_n	1868	(1637 .. 2132)	18.2	(13.9 ..23.8)	(x 10^{-6} cm/s)
fu_{cell}	0.2	(0.15 .. 0.237)	0.67	(0.63 ..0.7)	no units
Cl_{uptake} 1b1 (6.0)	2.0	(1.7..2.4)	0.77	(0.72..0.81)	(x 10^{-6} ml/s)
Cl_{uptake} 1b1 (7.4)	2.6	(2.3..3.0)	0.38	(0.34..0.41)	(x 10^{-6} ml/s)
Cl_{uptake} 1b3 (6.0)	0.59	(0.4..0.88)	0.38	(0.34..0.43)	(x 10^{-6} ml/s)
Cl_{uptake} 1b3 (7.4)	1.1	(0.85..1.35)	0.25	(0.22..0.28)	(x 10^{-6} ml/s)

Reported values represent the model derived estimate (95% CI)

DMD Fast Forward. Published on July 14, 2014 as DOI: 10.1124/dmd.114.058032
This article has not been copyedited and formatted. The final version may differ from this version.

Table 3 Predicted Transwell MDCK-LE permeabilities at multiple pH

	PF-049			PF-051	
pH	Predicted	Experimental	Predicted	Experimental	Units
5.5	10.18	7	0.89	1.4	($x\ 10^{-6}$ cm/s)
6.5	1.87	2.4	0.81	1.14	($x\ 10^{-6}$ cm/s)
7.4	1.06	1.4	0.80	0.46	($x\ 10^{-6}$ cm/s)

DMD Fast Forward. Published on July 14, 2014 as DOI: 10.1124/dmd.114.058032
This article has not been copyedited and formatted. The final version may differ from this version.

Table 4 Observed versus predicted steady state *Kpuu* in muscle and pancreas

	Kpuu (observed)	Kpuu (predicted)
PF-049		
Pancreas	0.25	0.24
Muscle		
Bulk	0.1	ND[a]
Slow-twitch oxidative	ND[b]	0.089
Fast-twitch oxidative	ND[b]	0.084
Fast twitch oxidative	ND[b]	0.055
PF-051		
Pancreas	0.07	0.22
Muscle		
Bulk	0.07	ND[a]
Slow-twitch oxidative	ND[b]	0.074
Fast-twitch oxidative	ND[b]	0.068
Fast twitch oxidative	ND[b]	0.041

[a] – *Kpuu* was not predicted for bulk muscle as relative fractions of different muscle types were unknown. [b] – *Kpuu* was experimentally determined only as bulk muscle.

Figure 1

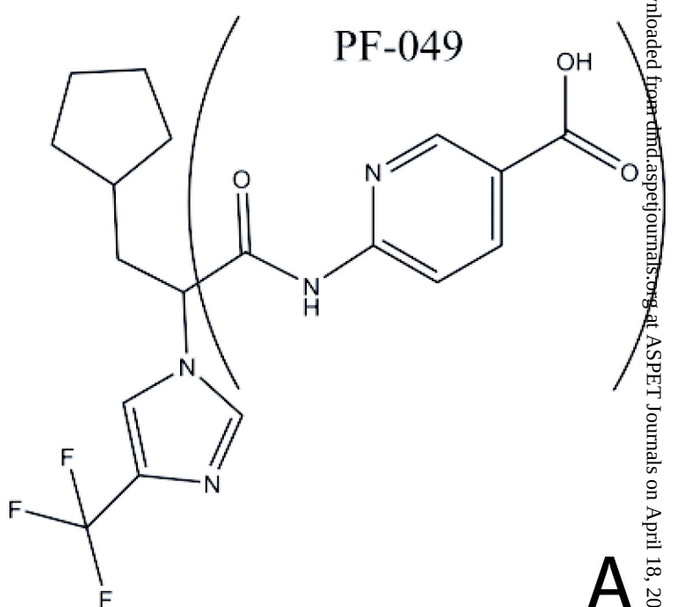

A

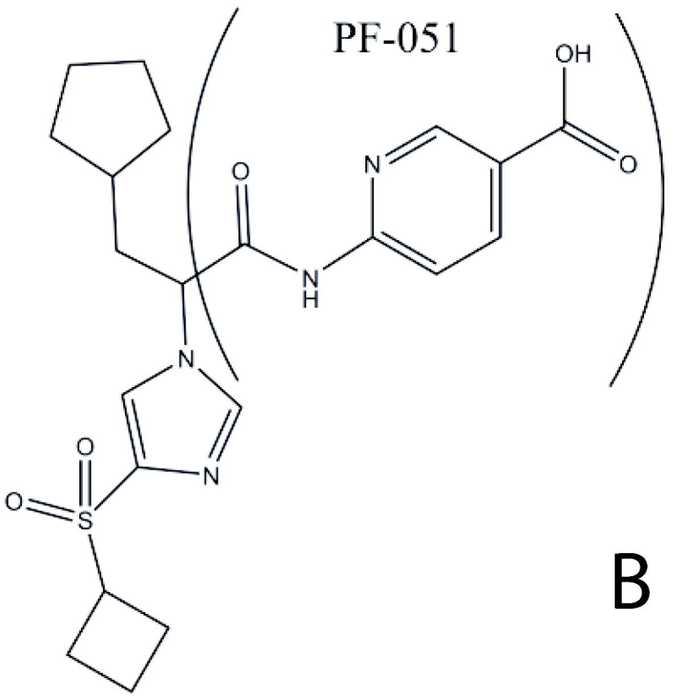

B

MW	396	447
pKa	3.5	3.5
$cLogD_{6.5}$	0.009	0.514
$cLogD_{7.4}$	-0.238	0.268
cLogP	3.66	3.34
TPSA	97.1	139

Figure 2

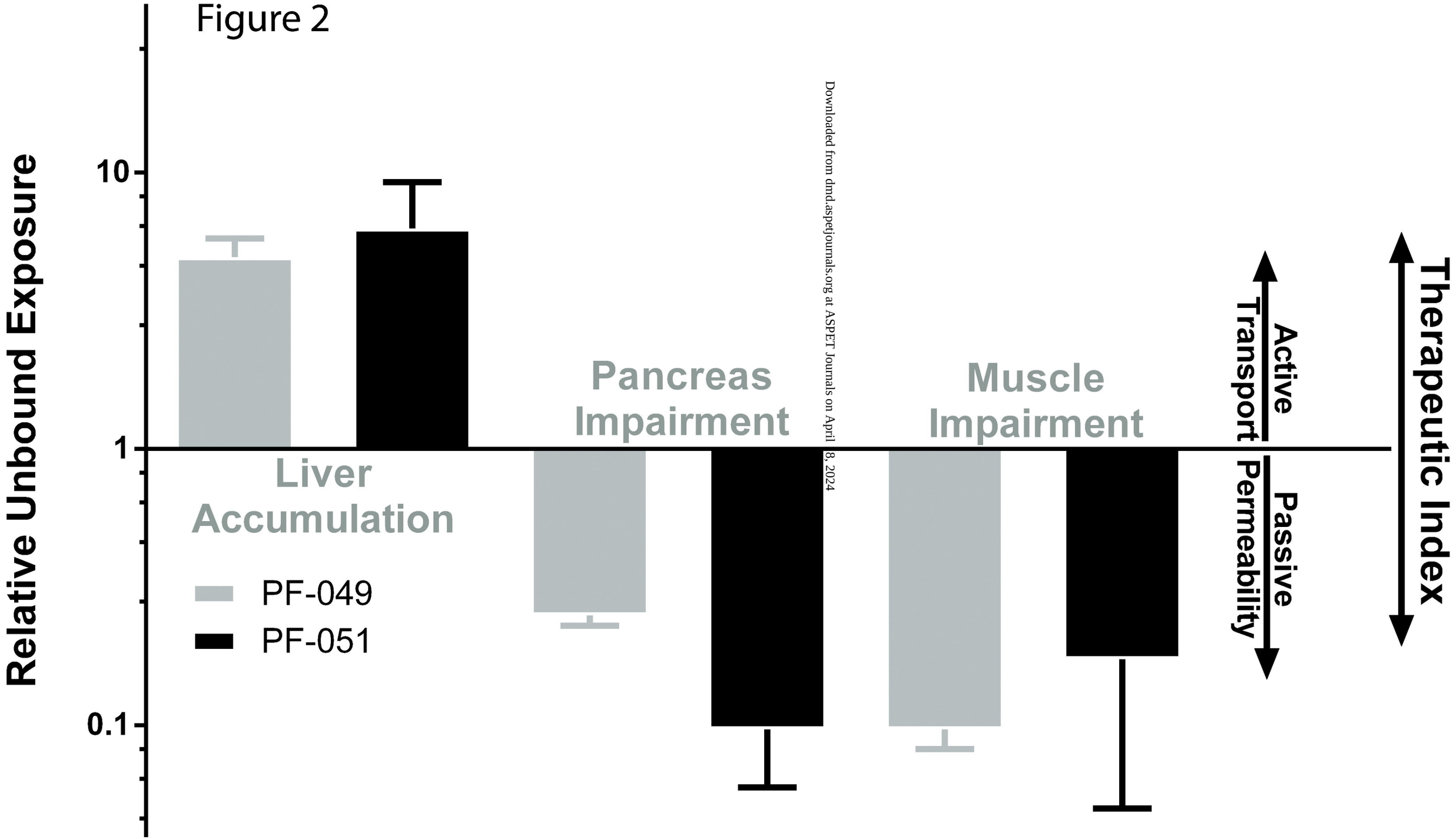

Figure 3

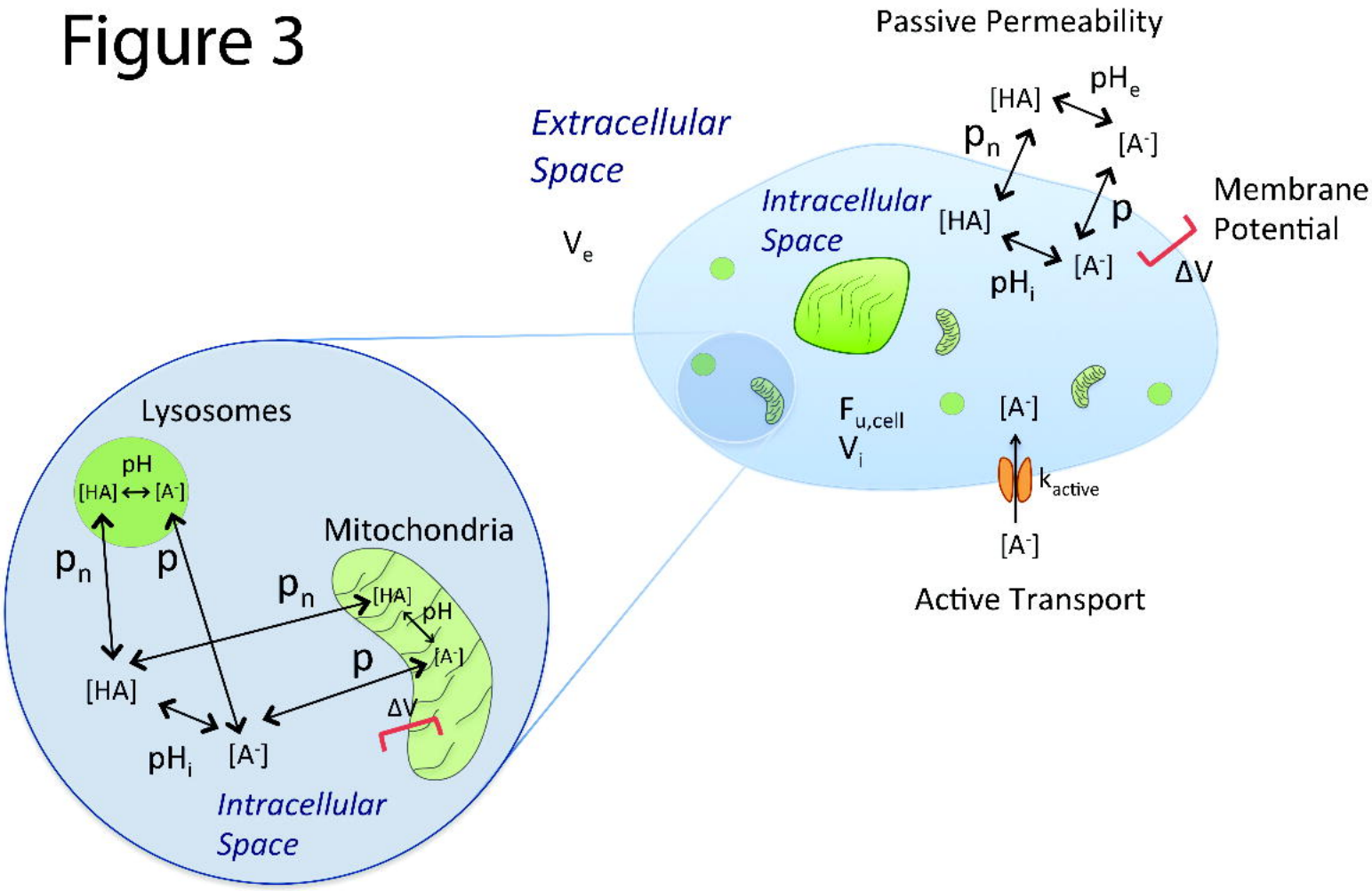
Passive Permeability
Extracellular Space
V_e
Intracellular Space
[HA]
pH_e
p_n
[A⁻]
p
Membrane Potential
[HA]
[A⁻]
pH_i
ΔV
$F_{u,cell}$
V_i
[A⁻]
k_{active}
[A⁻]
Active Transport
Lysosomes
pH
[HA] ↔ [A⁻]
p_n
p
Mitochondria
p_n
[HA]
pH
[A⁻]
p
[HA]
ΔV
pH_i
[A⁻]
Intracellular Space

Figure 4

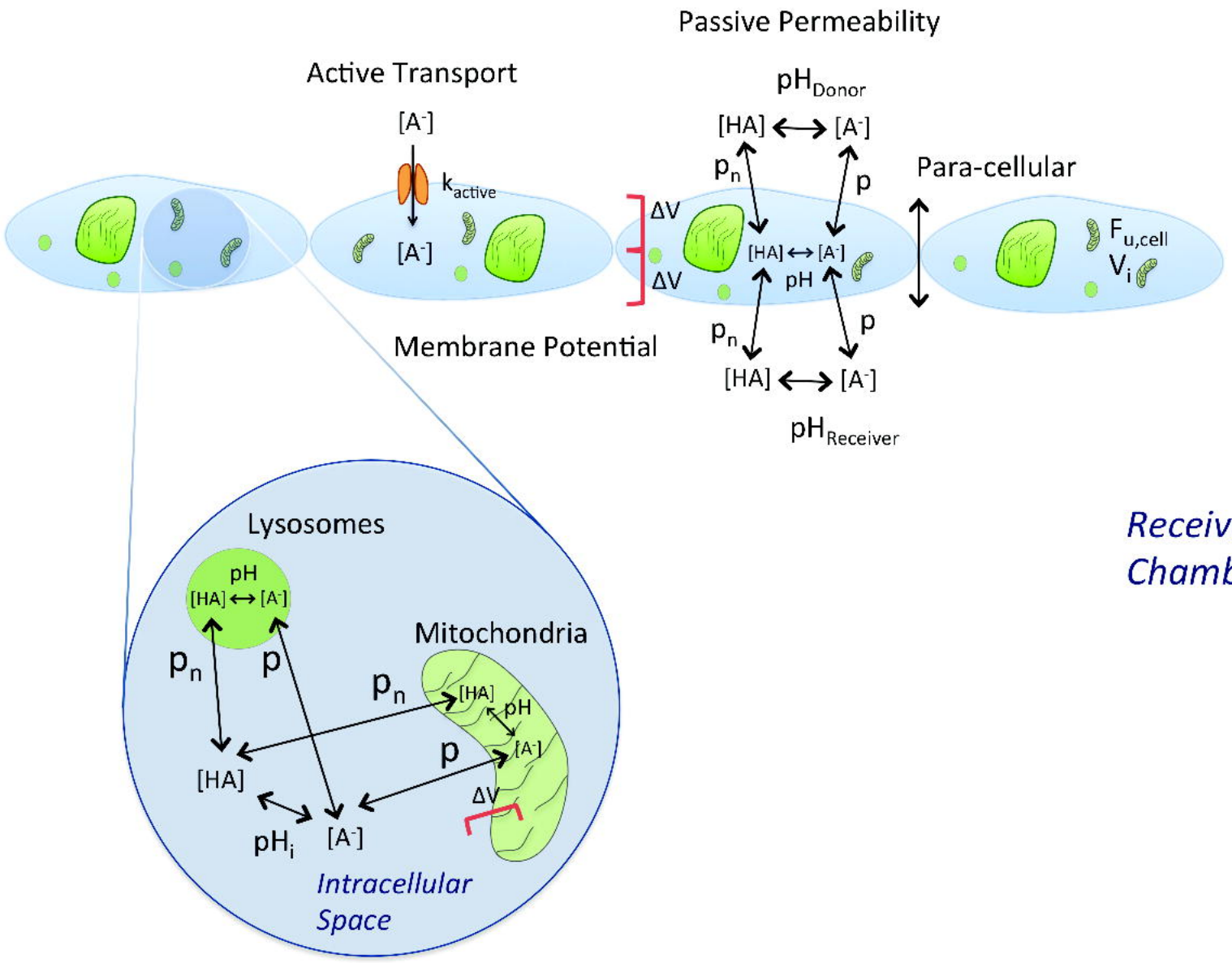
Donor Chamber
Passive Permeability
Active Transport
pH_{Donor}
$[A^-]$
[HA] ↔ $[A^-]$
k_{active}
p_n
p
Para-cellular
ΔV
ΔV
$F_{u,cell}$
V_i
$[A^-]$
[HA] ↔ $[A^-]$
pH
Membrane Potential
p_n
p
[HA] ↔ $[A^-]$
$pH_{Receiver}$
Receiver Chamber
Lysosomes
pH
[HA] ↔ $[A^-]$
Mitochondria
p_n
p
p_n
[HA]
pH
$[A^-]$
p
[HA]
ΔV
pH_i
$[A^-]$
Intracellular Space

DMD Fast Forward. Published on July 14, 2014 as DOI: 10.1124/dmd.114.058032
This article has not been copyedited and formatted. The final version may differ from this version.

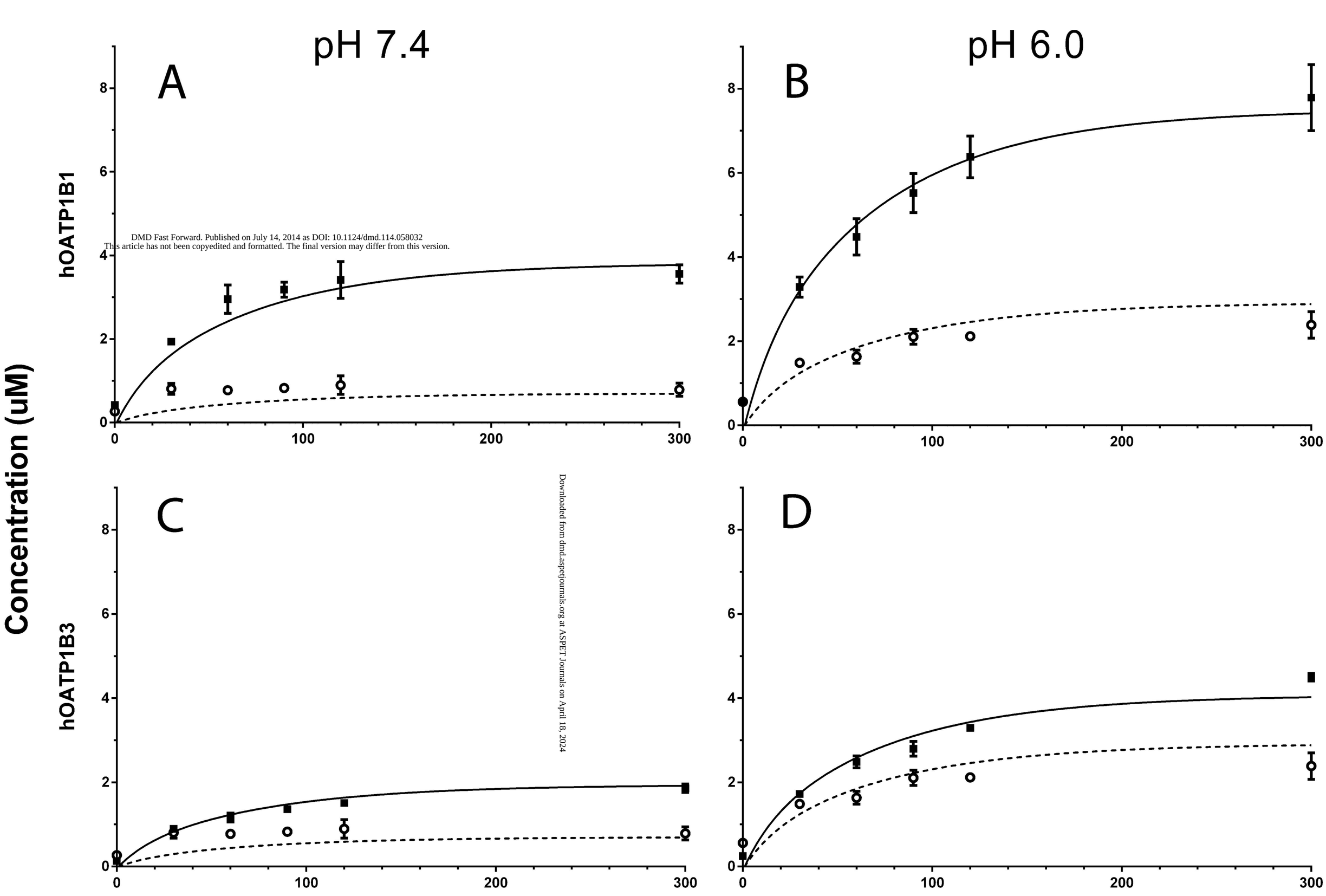

Figure 5

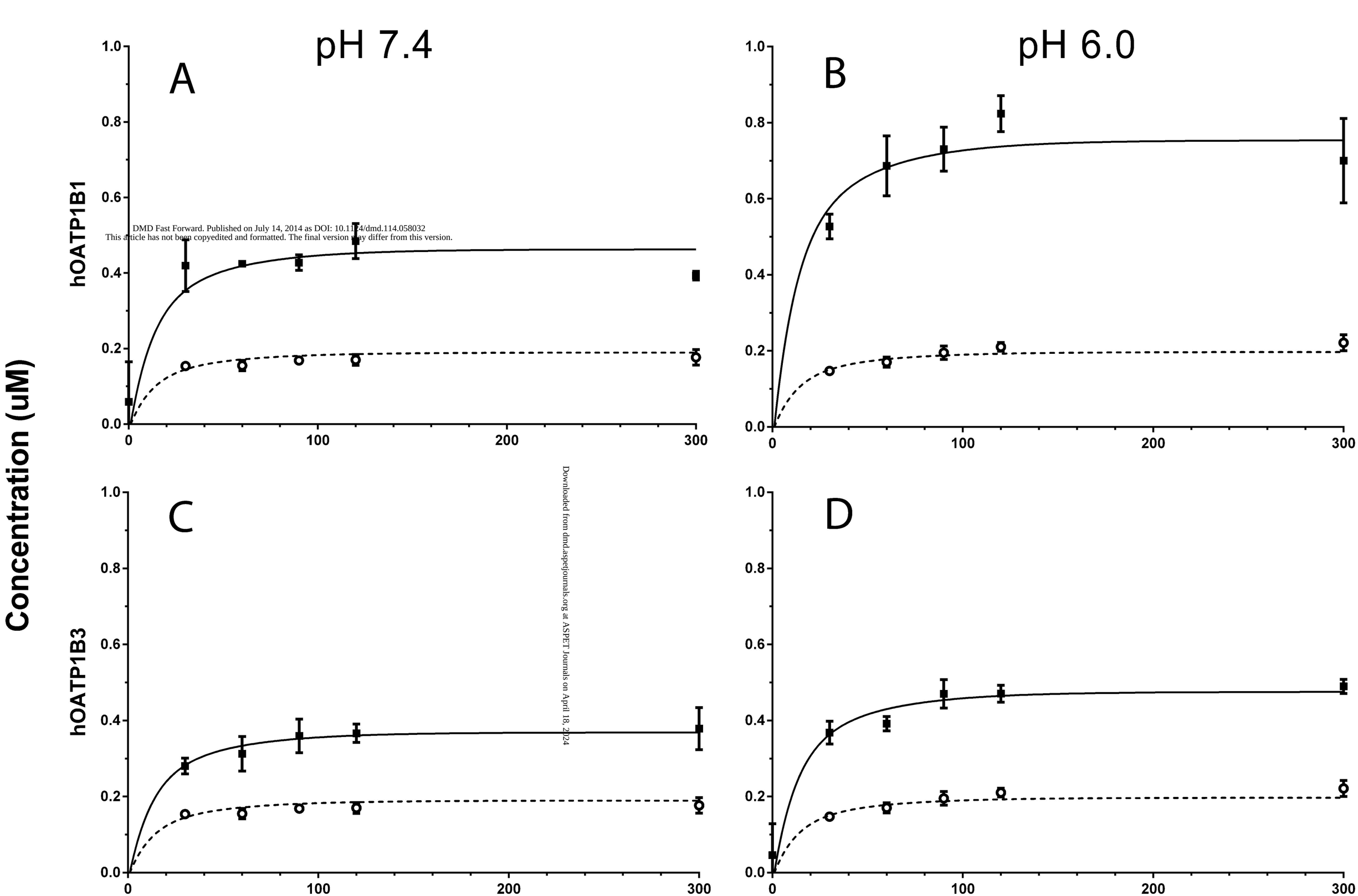

Figure 6

DMD Fast Forward. Published on July 14, 2014 as DOI: 10.1124/dmd.114.058032
This article has not been copyedited and formatted. The final version may differ from this version.

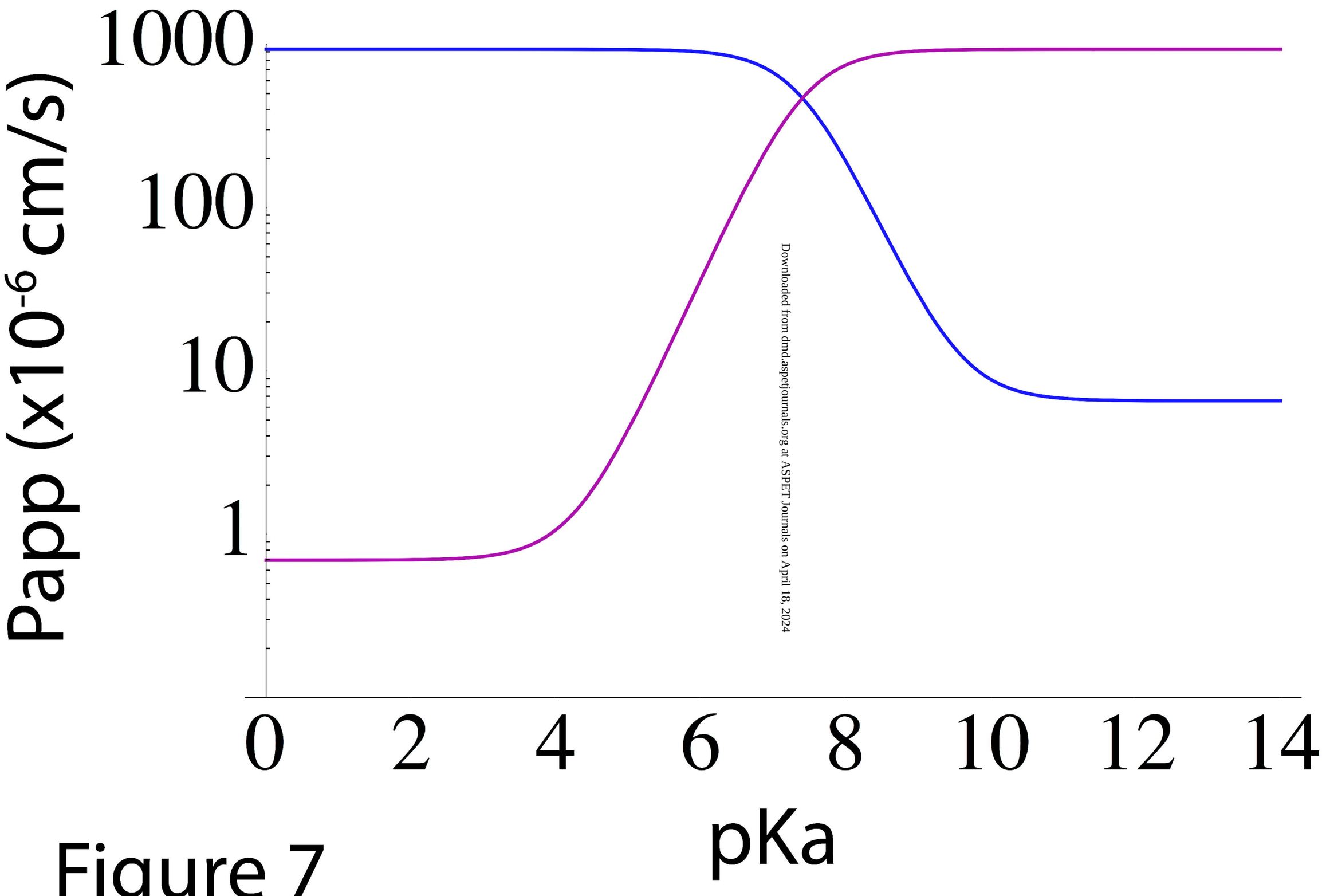

Figure 7

Figure 8